Chemical Engineering Journal 262 (2015) 785–793

Contents lists available at ScienceDirect

Chemical Engineering Journal

journal homepage: www.elsevier.com/locate/cej

Effect of channel size on mass transfer during liquid–liquid plug flow in small scale extractors

Dimitrios Tsaoulidis, Panagiota Angeli *

Department of Chemical Engineering, University College London, Torrington Place, London WC1E 7JE, UK

HIGHLIGHTS

- Effect of channel size on mass transfer in liquid–liquid extraction in small channels.
- High mass transfer coefficients in small channel extractions with ionic liquids.
- Use of ionic liquids as substitutes to organic solvents in the extraction of uranium.
- Development of numerical model to predict mass transfer in liquid–liquid extraction.

ARTICLE INFO

Article history:
Received 27 June 2014
Received in revised form 3 October 2014
Accepted 5 October 2014
Available online 13 October 2014

Keywords:
Liquid–liquid
Plug flow
Ionic liquid
Extraction
Spent nuclear fuel reprocessing

ABSTRACT

In this paper the effect of channel size on the mass transfer characteristics of liquid–liquid plug flow was investigated for capillaries with internal diameter ranging from 0.5 to 2 mm. The extraction of $\{UO_2\}^{2+}$ ions from nitric acid solutions into TBP/IL mixtures, relevant to spent nuclear fuel reprocessing, was studied for different residence times, dispersed phase fractions, and mixture velocities. It was found that extraction efficiencies increased as the channel size decreased. For a given channel length and for all channel sizes, an increase in mixture velocity decreased the extraction efficiency. The overall mass transfer coefficients ($k_L\alpha$) for all channels varied between 0.049 and 0.29 s^{-1} and decreased as the channel size increased. The evolution of the $k_L\alpha$ along the extraction channel showed a decreasing trend for all the channel sizes. The experimentally obtained mass transfer coefficients were compared with existing models for liquid–liquid and gas–liquid segmented flows from the literature. The results showed good agreement with the empirical correlation proposed for a liquid–liquid system. A finite element model was developed that solved the velocity and concentration fields in the channel for both phases considering a unit cell (one plug and one slug) with periodic boundary conditions at the inlet and the outlet. The model used experimental data for the geometric characteristics of the plug flow and predicted reasonably well the experimentally measured extraction efficiencies (with mean relative error of 11%).
© 2014 The Authors. Published by Elsevier B.V. This is an open access article under the CC BY license (http://creativecommons.org/licenses/by/3.0/).

1. Introduction

Two-phase, liquid–liquid systems find many applications in the process and chemical industries including solvent extraction, catalysis, polymerization, and nitration [1]. Solvent extraction in particular is one of the main processes in reprocessing of the spent fuel from a nuclear reactor. Commonly, uranium(VI) (and plutonium(IV)) are recovered from nitric acid solutions of the spent nuclear fuel through the PUREX process, with mixtures of organic solvents with tributylphosphate (TBP) as extractant [2]. Organic solvents, however, are flammable, volatile, and suffer from radiolysis, thus posing problems to the plants and threats to the environment. Ionic liquids are considered as alternative candidates to conventional organic solvents and have found applications in catalytic reactions, separation processes, and synthesis [3]. In general, ionic liquids are salts composed from ions that have low melting points (below 100 °C), while many of them are liquid even at room temperature [4]. They have very good physical characteristics such as, negligible vapour pressure and high thermal stability in normal operating conditions, while their high resistance to radiation makes them suitable for spent nuclear fuel reprocessing. A popular anion choice for synthesizing hydrophobic ionic liquids that are chemically and thermally more stable and of lower viscosity compared to the majority of ionic liquids, is the bis(trifluoromethylsulfonyl)imide anion $[(CF_3SO_2)_2N]^-$ (abbreviated to $[Tf_2N]^-$) [5]. The production of the ionic liquids can be expensive though, and thus prevent their extensive use in large-scale

* Corresponding author. Tel.: +44 (0) 20 7679 3832; fax: +44 (0) 20 7383 2348.
E-mail address: p.angeli@ucl.ac.uk (P. Angeli).

http://dx.doi.org/10.1016/j.cej.2014.10.012
1385-8947/© 2014 The Authors. Published by Elsevier B.V.
This is an open access article under the CC BY license (http://creativecommons.org/licenses/by/3.0/).

Nomenclature

A	cross sectional area [m^2]
$[C]_{aq,init}$	initial concentration of dioxouranium(VI) in aqueous phase [mol L^{-1}]
$[C]_{aq,fin}$	final concentration of dioxouranium(VI) in aqueous phase [mol L^{-1}]
$[C]_{aq,eq}$	concentration of dioxouranium(VI) in aqueous phase at equilibrium [mol L^{-1}]
D	diffusion coefficient [m^2 s^{-1}]
E_{eff}	extraction efficiency [%]
ID	internal diameter of the microchannel [m]
K_U	distribution coefficient of dioxouranium(VI) [dimensionless]
k_L	overall mass-transfer coefficient [m s^{-1}]
$k_L\alpha$	overall volumetric mass transfer coefficient [s^{-1}]
L	length [m]
Q	volumetric flow rate of fluid [m^3 s^{-1}]
t	residence time [s], $t = u_p/L_{ch}$
u	velocity [m s^{-1}]
V	volume [m^3]
w	width [m]

Greek letters

α	specific interfacial area [m^2 m^{-3}]
δ	film thickness [μm]
ε	volume fraction [dimensionless]
μ	dynamic viscosity [kg m^{-1} s^{-1}]
ρ	density [kg m^{-3}]
τ	residence time [s], $\tau = V_{ch}/Q_{mix}$

Subscripts

c	continuous
cap	cap
ch	channel
d	dispersed phase
eff	efficiency
film	film
g	gas
mix	mixture
IL	ionic liquid
p	plug
UC	unit cell

systems. The application of intensified small scale units in extraction processes would reduce the amount of solvent required and associated costs, and would make economically viable the use of ionic liquids.

Mixing and mass transfer are significantly enhanced in small scale two-phase contactors, despite the absence of turbulence, as a result of high specific interfacial areas, increased molecular diffusion through the thin fluid layers, improved radial mixing due to recirculation within phases [6], convection induced by surface tension gradients, and flow instabilities between the two immiscible phases [7]. The increased importance of interfacial and viscous forces in small channels, however, results in different patterns to those encountered in large scale systems [5], whose characteristics need to be studied as they affect mass transfer. One of the most common configurations in liquid–liquid flows is the plug (segmented) flow pattern, where drops of one liquid (plugs), with diameter larger than the channel diameter, are formed within the other liquid, while a thin film separates the plugs from the channel wall.

Operating small scale contactors with the high viscosity ionic liquids would bring in a number of challenges. In plug flow the size of the segments is among others an important parameter since it affects the interfacial area available for mass transfer and the intensity of the circulation patterns, and subsequently the heat and mass transfer rates. In small-channel flows, both the dispersed and the continuous phase properties influence the formation of the plug. Studies on the effect viscosity on the formation of the plugs and on the mixing inside the segments has been performed both numerically [8,9] and experimentally [10–12], however the results are limited and not conclusive. The use of high viscous liquids as continuous phase is also expected to affect the magnitude of the film that surrounds the dispersed plug, which is related to the Ca number, and the internal circulation within the dispersed plug which is affected by the shear stress induced by the liquid film. Studies on internal circulation in liquid–liquid systems that involve ionic liquids have been limited so far. Using numerical simulations, Kashid et al. [13], showed that the circulation patterns in the two phases are independent of viscosity. Dore et al. [6,14] investigated the mixing patterns in aqueous-ionic liquid systems and the internal circulation within the continuous or dispersed aqueous phase in plug flow, using micro-Particle Image Velocimetry (μ-PIV). It was found that the circulation within the aqueous segments is strongly related to the flow rates and the size of the segments. Scheiff et al. [15] studied the internal circulation within ionic liquid segments in an organic-ionic liquid two-phase flow. They found that the internal circulation within the ionic liquid segments is slower than in aqueous segments by a factor of 2–10. Moreover, they showed that circulation velocity was higher when the ionic liquid was the continuous phase than when it was the dispersed.

To evaluate the performance of two-phase small scale separators (gas–liquid or liquid–liquid) the mass transfer coefficients need to be known. A number of models have been developed for gas–liquid Taylor bubble (plug) flow based on both empirical correlations, and on film and penetration theory. These models provide estimates of the mass transfer coefficient in the continuous liquid phase, while the mass transfer resistance in the gas phase is considered negligible. The individual contributions of the caps of the bubbles and of the fully developed film separating the bubbles from the channel wall are estimated. Bercic and Pintar [16] proposed a model for the calculation of the mass transfer coefficient in small channels (Eq. (1)), that includes only the contribution of the caps because of the rapid saturation of the film.

$$k_L\alpha = \frac{0.111 u_p^{1.19}}{((1-\varepsilon_d)L_{UC})^{0.57}} \quad (1)$$

However, the absence of any parameter related to the channel size limits the application of the model to different two-phase systems.

Van Baten and Krishna [17] and Irandoust and Anderson [18] included in their models the contributions of both bubble caps and film (Eq. (2)). Van Baten and Krishna [17] evaluated the contribution of the caps (Eq. (3)) according to the Higbie penetration theory, whilst the transfer through the film (Eqs. (4) or (5)) was obtained based on mass transfer in a falling film in laminar flow. The mass transfer rates predicted by the correlations agreed well with the results from CFD (computational fluid dynamics) simulations.

$$k_L\alpha = k_{L,cap}\alpha_{cap} + k_{L,film}\alpha_{film} \quad (2)$$

$$k_{L,cap}\alpha_{cap} = \left[2\frac{\sqrt{2}}{\pi}\sqrt{\left(\frac{D_c u_p}{ID}\right)}\right]\left[\frac{4}{L_{UC}}\right] \quad (3)$$

$$k_{L,film}\alpha_{film} = \left[\frac{2}{\sqrt{\pi}}\sqrt{\frac{D_c u_p}{L_{film}}}\right]\left[\frac{4L_{film}}{IDL_{UC}}\right] \text{ for Fo} < 0.1 \quad (4)$$

$$k_{L,film}\alpha_{film} = \left[3.41\frac{D_c}{\delta_{film}}\right]\left[\frac{4L_{film}}{IDL_{UC}}\right] \text{ for Fo} > 1 \quad (5)$$

$$Fo_{film} = \frac{D_c L_{film}}{u_p \delta_{film}^2} \quad (6)$$

Similarly, Vandu et al. [19] suggested a model based only on the contribution of the film.

$$k_L\alpha = C\sqrt{\frac{D_c u_g}{L_{UC}}}\frac{1}{ID} \quad (7)$$

An empirical correlation has been developed by Yue et al. [20] for two-phase systems without reaction in an attempt to improve the inaccurate predictions obtained by the model of van Baten and Krishna [17] in square mini-capillaries. Shao et al. [21] proposed a numerical model in which concentration was calculated in both phases simultaneously, whilst the computational domain and the geometric characteristics of the system (bubble size and film thickness) were determined from empirical correlations.

In liquid–liquid systems several parameters that affect the performance of the extractor (with or without chemical reaction) such as channel size, flow patterns, fluid properties, mixing, and flow orientation have been investigated [22–30]. A number of investigations have focused on the development of numerical and empirical models to describe the mass transfer for fixed interface location [13,31,32]. Harries et al. [33] developed a numerical model for liquid–liquid plug flow to investigate the hydrodynamics within both continuous and dispersed phase segments and the mass transfer of dissolved chemical species in both phases and across the interface. The model, where segmented flow was represented by two adjacent rectangular units with moving wall, predicted well their experimental results. A similar model has been developed by Kashid et al. [13], to investigate the flow patterns and the mass transfer with or without reaction between two consecutive segments with fixed location. Raimondi et al. [34] carried out numerical simulations of the mass transfer during liquid–liquid plug flow in square microchannels, where it was assumed that mass transfer did not deform the interface, enabling the hydrodynamics to be decoupled from the mass transfer.

An empirical correlation, based on dimensional analysis in PTFE capillaries was proposed by Kashid et al. [35], (Eq. (8)). In their studies however, the inlet geometry or the microchannel shape were not taken into account.

$$k_L\alpha\frac{L}{u_{mix}} = a\mathrm{Ca}^b\mathrm{Re}^c\left(\frac{ID}{L}\right)^d \quad (8)$$

For industrial application of small scale systems, increased throughputs are necessary. Scale out is often considered, where the number of small channels or units is increased. This can, however, require a prohibitively large number of small channels. An alternative approach would be to first increase throughput by increasing the channel sizes, while still preserving the benefits of small scale operation, such as laminar flows and well defined regular patterns, and then consider scale out. It is then important to understand and be able to predict the effect that the channel size has on the hydrodynamic and mass transfer characteristics of the two-phase system.

In this paper, the effect of channel size on the extraction of $\{UO_2\}^{2+}$ ions from nitric acid solutions into a TBP/ionic liquid mixture is studied during plug flow in small channels. The experimental mass transfer coefficients are compared against predictive literature models. In addition, a numerical finite element model is developed which solves for the hydrodynamics and mass transfer in both phases. The model predictions on amount of extraction are compared against the experimental findings.

2. Model formulation

The numerical model was developed to simulate the mass transfer of $\{UO_2\}^{2+}$ ions in the aqueous/ionic liquid system during plug flow. For the simulations a unit cell (one dispersed phase plug and one continuous phase slug) in 2-D axisymmetric cylindrical coordinates is used. The two-phase flow and the concentration profiles are considered symmetric over the channel axis, and only half of the unit cell is simulated. The whole computational domain is depicted in Fig. 1. The geometric characteristics, such as length of the plug and the slug and film thickness were chosen based on experimental findings.

In the model it was assumed that surface tension gradients and gravity are negligible. Both liquids were Newtonian, viscous and the flow was incompressible. It was also assumed that mass transfer does not affect the interface shape and the volume of the unit cell. The computational procedure followed two steps. First, the hydrodynamics of the system were determined by solving the velocity field (**u**) and the pressure for the two liquid phases using the Navier–Stokes and the continuity equations (Eqs. (9) and

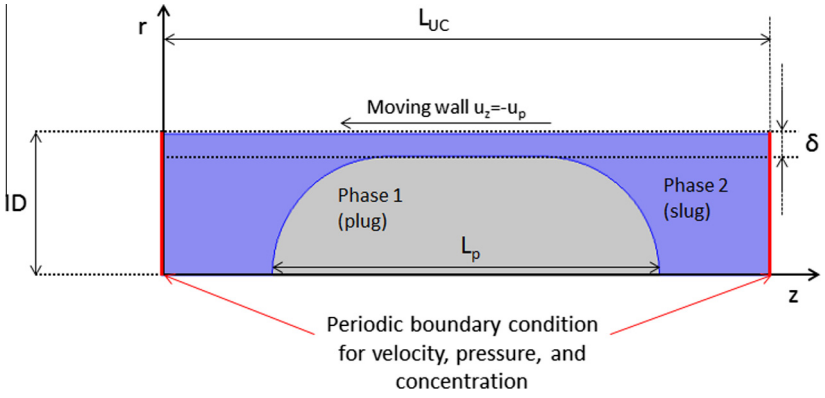

Fig. 1. Geometry and boundaries of the unit cell computational domain for the simulation of mass transfer in liquid–liquid plug flow.

(10)). Subsequently, the convection–diffusion equation (Eq. (11)) was solved in both phases.

$$\rho(\mathbf{u}\cdot\nabla)\mathbf{u} = \nabla\cdot\left[-\mathrm{PI} + \mu\left(\nabla\mathbf{u} + (\nabla\mathbf{u})^{\mathrm{T}}\right)\right] + \mathbf{F} \quad (9)$$

$$\rho\nabla\cdot\mathbf{u} = 0 \quad (10)$$

$$\frac{\partial c_i}{\partial t} + \nabla\cdot(D_i\nabla c_i + \mathbf{u}c_i) = 0 \quad (11)$$

The position and the shape of the plug in the computational domain remained fixed, while the wall of the channel was moving with a constant velocity equal to the plug velocity, u_p, but with direction opposite to the flow. The plug has higher velocity than the mixture velocity because of the thin film on the wall; for the simulations the experimental plug velocity is used. The following boundary conditions were applied to the fluid flow equations:

(1) axial and radial velocity of the channel wall equal to $u_z = -u_p$ and $u_r = 0$, respectively;
(2) no-slip boundary condition at the channel wall;
(3) equal stresses at the interface between the two phases. This approach is correct when the plug geometry accurately represents the equilibrium state of the plug where forces are balanced.

For the mass transfer equation a boundary condition was applied to satisfy the flux continuity at the interface, while zero flux was set at the channel wall. Periodic boundary conditions are used at the front and the back of the computational domain for the velocity, the pressure, and the concentration (see Fig. 1).

All simulations were performed with a commercial finite element software (Comsol Multiphysics 4.4.). The hydrodynamic equations for both liquid domains were solved in a steady-state mode to establish the velocity and pressure profiles, while the mass transfer equations, one for each phase, were solved in a transient manner to represent mass transfer during the movement of the plug along the channel. A free triangular mesh was used in the simulations in the whole computational domain, which was additionally refined along the interface and the channel wall, where the characteristic length scales are very short and the concentration gradients are steep. Sensitivity analysis was carried out to establish the grid size needed for grid independent mass transfer. It was found that the minimum and the maximum element sizes along the interface should be 0.4 μm and 3 μm, respectively, for the 1 mm and 2 mm ID channels and 0.1 μm and 1.6 μm, respectively, for the 0.5 mm ID channel. In the subdomains (phases 1 and 2) the grid size should be less than 32 μm. It was also found that a time step equal to 0.05 s was satisfactory since there were small discrepancies in concentration compared to shorter time steps. Finally, in order to avoid very large instantaneous flux across the interface, a step function was added to the model.

3. Experimental setup and procedure

A schematic of the experimental setup used for the continuous extraction experiments is shown in Fig. 2. The two phases were two immiscible solutions, i.e. HNO_3/U(VI) and 30% v/v TBP/ionic liquid. The HNO_3/U(VI) solutions were prepared in the UCL laboratory from HNO_3 (65%) solution of general purpose grade by Fisher Scientific and dioxouranium(VI) nitrate hexahydrate $UO_2(NO_3)_2\cdot 6H_2O$ by Sigma–Aldrich. The 30% v/v TBP/ionic liquid solution was prepared by using tributylphosphate (TBP) (Sigma–Aldrich) and an ionic liquid 1-methyl-3-butyl-imidazolium bistriflimide, i.e. $[C_4mim][NTf_2]$ ($\mu = 0.052$ kg m^{-1} s^{-1}, $\rho = 1420$ kg m^{-3}) which was prepared at the QUILL research centre by following a standard procedure. The experiments were carried out at atmospheric pressure and at room temperature ($T = 298$ K). The initial concentration in the aqueous nitric acid solution was set to 3 M for all the experiments, whilst the concentration of $\{UO_2\}^{2+}$ in nitric acid was 0.05 M. Two high precision pumps (KdScientific) were used to introduce the two liquids into the main test section via a T-junction mixer. The mixer was made of FEP with all branches having always the same internal diameter as that of the main channel. The extraction experiments were carried out in circular channels

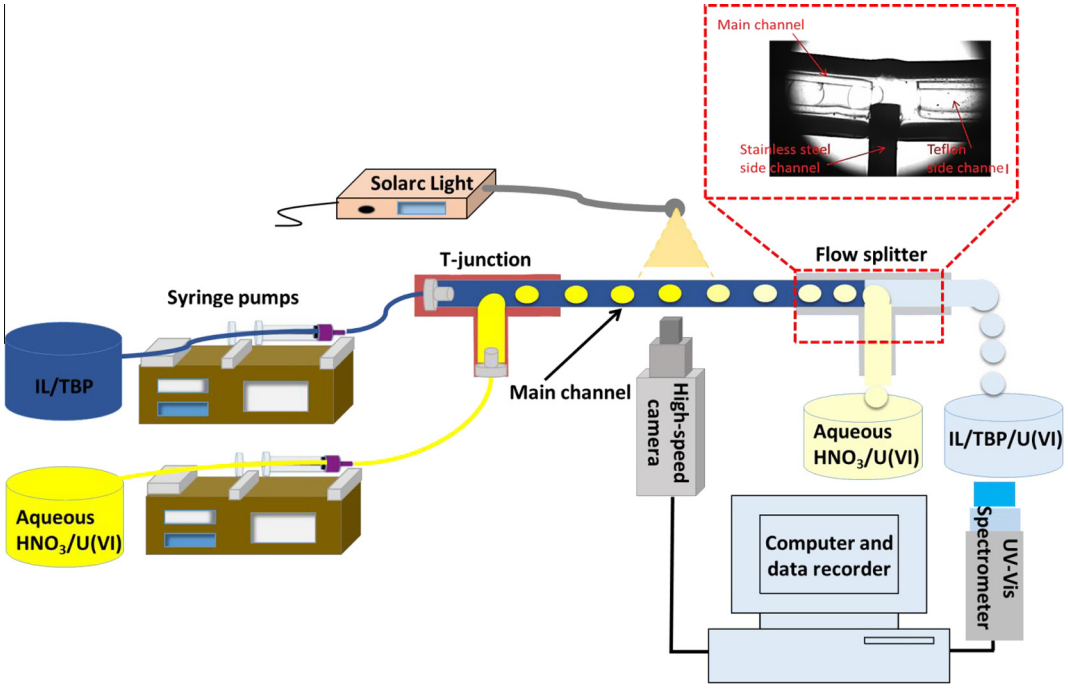

Fig. 2. Schematic of the experimental setup.

with different internal diameters, i.e. 0.5 mm, 1 mm, and 2 mm, whilst the lengths varied from 10 cm to 31.5 cm. Experiments were carried out for total volumetric flow rates (Q_{mix}) varying from 7 to 340 $cm^3\ h^{-1}$, and input aqueous phase volume fraction ε_d from 0.5 to 0.67. At all experimental conditions plug flow was established with the aqueous phase (HNO_3 solution) flowing as non-continuous (dispersed) plugs within the TBP/IL phase (continuous) which was in contact with the channel wall. The flow was visualised with a high-speed camera (Photron APX) and was illuminated with a 60 W continuous arc lamp. 2MP 10 bits images were acquired at 2000–4000 Hz (depending on the total flow rate) that were stored in a computer for further analysis. At the end of the test section the two phases were separated online with a flow splitter made in-house, which comprised of two side channels (made of stainless steel and PFA) that had different wettabilities for the two phases [36]. The internal diameter and the length of the side channels were chosen to enable control of the pressure difference between the two phases due to pressure losses in each phase and the Laplace pressure of the interface (similar to [37]). Phase separation was possible with this configuration for all flow rates shown, where pure ionic liquid was obtained from the PFA outlet and nitric acid solution from the stainless steel outlet. The amount of $\{UO_2\}^{2+}$ transferred from the aqueous phase was measured in the ionic liquid phase with a UV–Vis spectrometer (USB2000+, from Ocean Optics). Since the ionic liquid used in this work was hygroscopic (i.e. it absorbs small amounts of water), it was saturated with nitric acid solution before the experiments. Viscosity measurements were performed in a digital Rheometer DV-III Ultra (Brookfield). The experimental error was estimated by taking into account the errors in the initial concentration of uranium in the nitric acid solution (~2%) and in the concentration of $\{UO_2\}^{2+}$ in the ionic liquid phase as measured by the UV–Vis spectrometer (3–4.9%).

4. Results and discussion

Two parameters were used to characterise the mass transfer performance of the small scale extractor, i.e. the extraction efficiency ($\%E_{eff}$) (Eq. (12)) and the overall volumetric mass transfer coefficient ($k_L\alpha$) (Eq. (13)).

$$\%E_{eff} = \frac{[C]_{aq,fin} - [C]_{aq,init}}{[C]_{aq,eq} - [C]_{aq,init}} \tag{12}$$

$$k_L\alpha = \frac{1}{\tau} \ln\left(\frac{[C]_{aq,eq} - [C]_{aq,init}}{[C]_{aq,eq} - [C]_{aq,fin}}\right) \tag{13}$$

The effects of residence time, mixture velocity, and channel size on ($\%E_{eff}$) and $k_L\alpha$ are discussed below. At all experimental conditions studied, there was a thin film of the continuous phase separating the aqueous plug from the wall, which indicates that the entire plug surface was available for mass transfer. In cases where the film is absent, only the caps of the plug are available for mass transfer and the interfacial area reduces by 3–4 times [38].

Equilibrium extractions were also performed at room temperature with equal volumes of TBP/[C_4mim][NTf_2] (30%, v/v) and HNO_3/dioxouranium(VI) to estimate the distribution coefficient (K_U) (Eq. (14)). Mechanical shaking was applied for 3 h before the two phases were separated.

$$K_U = \frac{C_{aq,init} - C_{aq,eq}}{C_{aq,eq}} \tag{14}$$

Studies of dioxouranium(VI) extraction from nitric acid solutions to ionic liquids suggest different mechanisms for the extraction i.e. cation exchange, anion exchange and solvation, depending on the nature of extractant, concentration of counteranion, structure of the ionic liquid and the aqueous phase composition [39,40]. In the current study, where TBP is used as extractant, and the nitric acid concentration is 3 M, the extraction proceeds via an anion exchange mechanism.

$$UO_2^{2+} + 3NO_3^- + 2TBP + Tf_2N^- \leftrightarrow [UO_2(NO_3)_3(TBP)_2]^{2-} + Tf_2N^-$$

4.1. Extraction efficiency

The effect of mixture velocity on the mass transfer performance of the device can be seen in Fig. 3 for the three different channel sizes. The length of the channels was in all cases equal to L_{ch} = 10.5 cm. The results illustrate that for a given channel size as the mixture velocity increases the extraction efficiency decreases, and that for the same mixture velocity the extraction efficiency is always higher as the channel size decreases.

An increase in mixture velocity decreases the residence time available for mass transfer. At the same time, as the mixture velocity increases, the recirculation time within the plugs increases and consequently the mixing becomes more intense. In addition, the specific interfacial area available for mass transfer was found to be affected by both the mixture velocity and the channel size. For a given channel size, as the mixture velocity increases the interfacial area available for mass transfer also increases. This is because at higher mixture velocities shorter plugs are formed at the inlet due to the rapid penetration of one phase into the other [36]. Moreover, for a given mixture velocity the interfacial area available for mass transfer decreases as the channel size increases, because the plugs in the larger channels were found to be longer; thus a smaller number of segments is available in large channel compared to a small one for mass transfer. Considering two hemispherical caps in the front and back end of the plug the interfacial area depending on the Ca number can be calculated from [34]

$$\alpha_p = \frac{\pi w_p(L_p - w_p) + \pi w_p^2}{L_{UC} w_{ch}^2} \quad \text{for Ca} > 0.04 \tag{15}$$

$$\alpha_p = \frac{4 w_p(L_p - w_p) + \pi w_p^2}{L_{UC} w_{ch}^2} \quad \text{for Ca} < 0.04 \tag{16}$$

For example, in the case of the 0.5 mm ID channel, and using experimental plug geometric characteristics, it was found that there is an increase of ~45% on the interfacial area available for mass transfer for mixture velocity from 0.01 to 0.06 m s^{-1}, whilst the extraction efficiency falls by about 55%. The same effect is observed for the two bigger channel sizes as well. However, as the mixture velocity increases, the decrease in residence time seems to overcome any increases in mass transfer from improved mixing within the plugs and increased interfacial area and the extraction efficiency reduces.

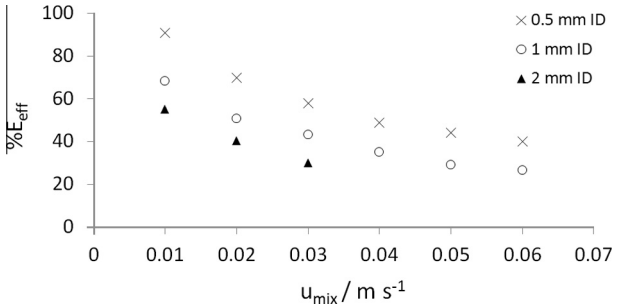

Fig. 3. Extraction efficiency ($\%E_{eff}$) of $\{UO_2\}^{2+}$ as a function of the mixture velocity for channel length L_{ch} = 10.5 cm and equal phase flowrates, in the 3 different channels.

The decrease of the extraction efficiency with increasing mixture velocity follows a non-linear trend. The extraction efficiency at high mixture velocities, i.e. 0.05 m s^{-1} and 0.06 m s^{-1}, does not change significantly in the case of the 0.5 and the 1 mm ID channel. Interestingly, even if the residence time is quite short at these mixture velocities (~2 s for 0.05 m s^{-1} and ~1.7 s in the case of 0.06 m s^{-1}) the extraction efficiency still reaches 40% and 30% for the 0.5 mm ID channel and the 1 mm ID channel, respectively.

To study the effects of residence time (i.e. $\tau = V_{ch}/Q_{mix}$) on mass transfer at the different channel sizes, the channel length was varied (from 10 to 31.5 cm) rather than the mixture velocity. Changes in the mixture velocity would alter the hydrodynamic characteristics of the two-phase flow, such as plug length and circulation patterns, which also affect mass transfer. In Fig. 4 the extraction efficiency ($\%E_{eff}$) of $\{UO_2\}^{2+}$ is plotted against the residence time at a constant mixture velocity of 0.03 m s^{-1} for equal flow rates of the two phases. As the residence time increases, the $\%E_{eff}$ also increases at all channel sizes. An extraction efficiency of >90% is achieved in the case of the 0.5 mm ID channel in less than 11 s, whilst in the 1 and 2 mm ID channels for the same time interval the $\%E_{eff}$ was <70% and <40%, respectively. It is worth noticing that a significant percentage of mass transfer occurs within the first 10 cm of the channel, which includes the plug formation region as well. Significant mass transfer at the inlet region has also been observed by Tan et al. [41] for gas–liquid systems. Depending on the channel size the increase in the extraction efficiency follows a different rate. In the 0.5 mm ID channel an increase of ~70% on the $\%E_{eff}$ is observed in a period of 7 s (from 4 to 11 s), whilst in the 1 and 2 mm ID channels for the same time interval the increase on the $\%E_{eff}$ is ~62% and ~33%, respectively. The short diffusional distances in the small channels improve mass transfer. Moreover, as the channel size decreases, the mixing becomes more intense within the aqueous plugs, since for the same conditions the plug size is smaller and the circulation faster [6,42]. The intense mixing enhances the mass transfer due to convection, and renews the interface between the two phases thus increasing the concentration gradients which improve the diffusive penetration of the transferred species. In addition, a decrease in plug size with decreasing channel size at the same mixture velocity and phase ratio results in more plugs and increases the interfacial area available for mass transfer.

4.2. Volumetric mass transfer coefficient ($k_L\alpha$)

The volumetric mass transfer coefficients were calculated for all conditions studied. As can be seen in Fig. 5, for a constant channel length of 10.5 cm and equal phase flowrates, an increase in the mixture velocity increases $k_L\alpha$ in all channel sizes. As discussed above, an increase in mixture velocity intensifies the mixing within the plugs and increases the interfacial area available for mass transfer. In addition, the mass transfer coefficients reduce as the channel size increases. This is attributed to more intense mixing and increased interfacial area at small channel sizes. For a certain mixture velocity, for example 0.01 m s^{-1}, the specific interfacial area decreases by about 66% by increasing the channel size from 0.5 to 1 mm ID and by 60% by increasing it from 1 to 2 mm ID. At the same conditions, as can be seen from Fig. 5 the $k_L\alpha$ decreases by about 50% from 0.5 to 1 mm ID, and about 33% from 1 to 2 mm ID channel.

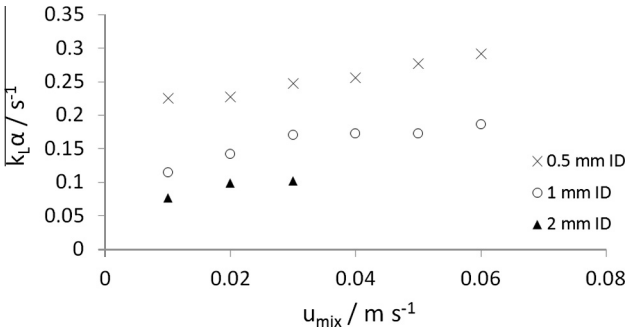

Fig. 5. Mass transfer coefficient as a function of the mixture velocity for channel length, L_{ch} = 10.5 cm, and equal phase flowrates in the 3 different channels.

However, when the mass transfer coefficients achieved at a constant residence time are plotted, different trends are observed for the different channel sizes as can be seen in Fig. 6. With increasing mixture velocity in the 0.5 mm ID channel the $k_L\alpha$ slightly increases, in the 1 mm ID channel it remains almost constant, while in the 2 mm ID channel it reduces. These differences are attributed to the different circulation patterns and mixing intensity, as well as the film thickness and plug length in the different diameter channels.

The evolution of the mass transfer coefficient ($k_L\alpha$) along the channel at a constant mixture velocity (u_{mix} = 0.03 m s^{-1}) also seems to depend on channel size (Fig. 7). For these measurements three different channel lengths were used for each channel size. For the 0.5 mm ID channel the mass transfer coefficient seems to remain almost constant along the first 20 cm and then it slightly decreases, whilst in the case of the 1 and 2 mm ID channels there is a decrease on the mass transfer coefficient for the whole length examined. This difference indicates that the mass transfer rate in the case of 0.5 mm ID channel is enhanced by the intense internal circulation. It can also be seen that for all channel sizes the mass transfer coefficient is larger for shorter channel lengths. For example, in the case of the 1 mm ID channel, the mass transfer coefficient in the 10 cm cannel is approximately 0.17 s^{-1}, whilst it is about 0.14 s^{-1} in the 20 cm channel. This indicates very good mass transfer close to the channel inlet where the phases join.

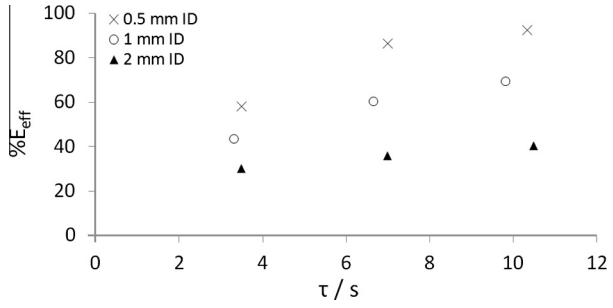

Fig. 4. Extraction efficiency ($\%E_{eff}$) of $\{UO_2\}^{2+}$ as a function of residence time at constant mixture velocity (u_{mix} = 0.03 m s^{-1}) and equal phase flowrates in the 3 different channels.

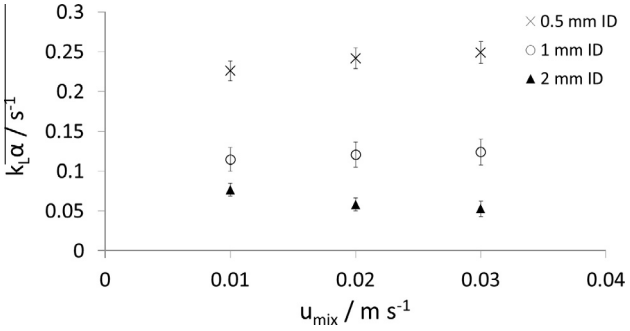

Fig. 6. Mass transfer coefficient as a function of the mixture velocity in the 3 different channels for equal phase flowrates, at the same residence time (~10 s).

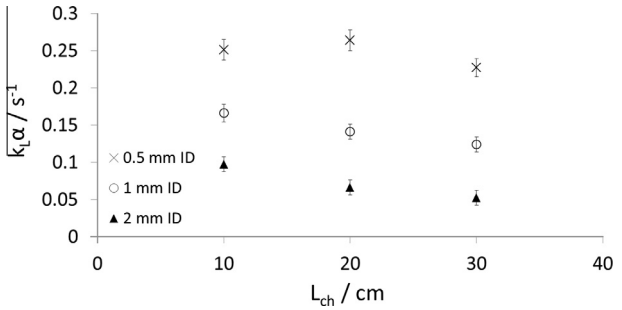

Fig. 7. Mass transfer coefficient as a function of the channel length at constant mixture velocity u_{mix} = 0.03 m s^{-1} and equal phase flowrates, in the 3 different channels.

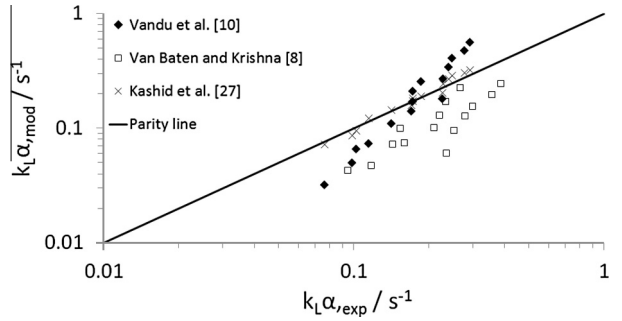

Fig. 8. Comparison of experimental $k_L\alpha$ with those predicted by correlations for all experimental conditions used.

In all cases and for similar conditions significant decrease of 50% in the mass transfer coefficients takes place when the channel size increases from 0.5 to 1 mm ID while with a further increase to 2 mm ID the decrease on the mass transfer coefficient is less pronounced, i.e. from 0.5 to 2 mm ID the decrease on $k_L\alpha$ is 72%.

4.3. Comparison of $k_L\alpha$ with literature correlations

The mass transfer coefficients obtained experimentally were compared with literature correlations (see Section 1) and the results are shown in Fig. 8. In general, the experimental results seem to agree well with the model proposed by Kashid et al. [35] for liquid–liquid plug flow in capillaries. The fitting parameters in Eq. (8) have been adjusted to the current experimental data (i.e., a = 0.44, b = −0.1, c = −0.65, d = −0.1) and the mass transfer coefficients are predicted within a range of errors from 0.6% to 13.2%. The highest errors were observed at high mixture velocities regardless of the channel size. The modified correlation seems to predict better the mass transfer coefficients in the 1 mm ID channel with a mean relative error of 3.5%.

The models of van Baten and Krishna [17] and Vandu et al. [19], developed based on gas–liquid bubble flows, showed little or no agreement with the experimental results. Van Baten and Krishna [17] developed their model over a wide range of parametric values (ID = 1.5–3 mm, L_{UC} = 15–50 mm). Their model underestimated the current mass transfer coefficients for all the channels. It is worth noting that in this work the length of the unit cells (L_{UC}) and the velocity of the dispersed phase (u_p) were one order of magnitude lower than those used by van Baten and Krishna [17]. In the model by Vandu et al. [19] (Eq. (7)), which was evaluated against data from different channel sizes (ID = 1–3 mm) and unit cell lengths (L_{UC} = 5–60 mm), the only contribution on the mass transfer coefficient is by the film. The $k_L\alpha$ obtained experimentally for 0.5 mm ID and 1 mm ID channel seem to fall within the predictions of their model (for C = 8.5), whilst mass transfer is underestimated in all cases for the 2 mm ID channel with a relative error from 40% to 60%. The discrepancies between the experimental results and the gas–liquid models may be attributed to the more complex hydrodynamics in the liquid–liquid systems. In addition, there is less resistance to mass transfer by diffusion within a gas plug compared to a liquid one.

4.4. Comparison of $k_L\alpha$ with the numerical model predictions

The numerical model developed in Section 2 was applied to the current system. The numerical results on the velocity fields and circulation patterns within the aqueous phase plugs have been validated against Particle Image Velocimetry measurements and good agreement was found [43]. The geometric characteristics of the flow needed for the simulations, i.e. film thickness (δ), length of unit cell (L_{UC}), and plug length (L_p) and the plug velocity (u_p), were derived from the high resolution images acquired during the experiments with the high-speed camera and are tabulated in Table 1. The residence time, ($t = u_p/L_{ch}$) selected for the simulations represents the time that an aqueous plug flows within the extraction channel. The properties of the fluids used for the simulations are shown in Table 2. The diffusion coefficients of $\{UO_2\}^{2+}$ in the TBP/IL (30%, v/v) mixture and in the aqueous nitric acid solution were selected based on literature data.

The effect of the channel size on extraction efficiency is shown in Fig. 9 as a function of residence time (t). Higher extraction efficiency can be achieved at a certain residence time for decreased channel size. The experimental results in this graph agree with the model within errors from 1.4% to 12.3%. However, in almost all cases the model underpredicts the experimental data. As was discussed above, significant mass transfer seems to take place at the beginning of the channel close to the inlet where the plug flow is not well formed yet. This is not accounted for in the model, which considers fully developed plug flow and would explain the underprediction.

Increased interfacial area can be achieved by changing the flowrate ratio between the two liquid phases. The effect of volume fraction ($\varepsilon_d = Q_d/Q_{mix}$) on the extraction efficiency is shown in Fig. 10 as a function of the residence time in the 1 mm ID channel with length L_{ch} = 10.5 cm. For these results the total flow rate of the mixture (Q_{mix}) was kept constant at 84.82 cm^3 h^{-1} (mixture velocity, u_{mix}, of 0.03 m s^{-1}), whilst the flow rate of the dispersed aqueous phase (Q_d) varied from 42.41 to 56.55 cm^3 h^{-1} which results in volume fractions (ε_d) increasing from 0.5 to 0.67. The change in ε_d does not limit the extraction of $\{UO_2\}^{2+}$ from the nitric acid solution because, according to the reaction stoichiometry, TPB is in

Table 1
Parametric values used in the numerical simulations.

ID [mm]	ε_d	L_{UC} [mm]	L_p [mm]	δ [μm]	u_p [m s^{-1}]
0.5	0.5	2.18	1.48	36.1	0.035
2	0.5	4.4	2.8	160.7	0.045
1	0.5	3.4	2.2	76.3	0.039
1	0.57	3.7	2.6	70.2	0.037
1	0.67	4.3	3.43	72.3	0.039

Table 2
Properties of the fluids used in the numerical simulations.

Properties	TBP/IL (30%, v/v)	HNO_3 (3 M)
Viscosity, μ (kg m^{-1} s^{-1})	0.029	0.001
Density, ρ (kg m^{-3})	1260	1070
Diffusion coefficient, D (m^2 s^{-1})	$7 \cdot 10^{-11}$ [44,45]	$7 \cdot 10^{-10}$ [44]

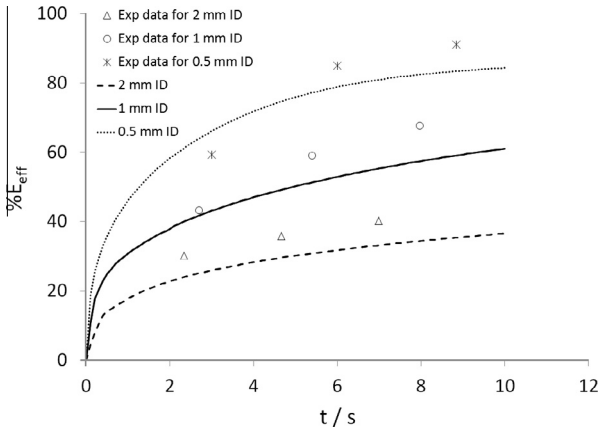

Fig. 9. Extraction efficiency ($\%E_{eff}$) of $\{UO_2\}^{2+}$, predicted by the numerical model, as a function of the residence time (t) in the 3 different channel sizes at constant mixture velocity u_{mix} = 0.03 m s^{-1}.

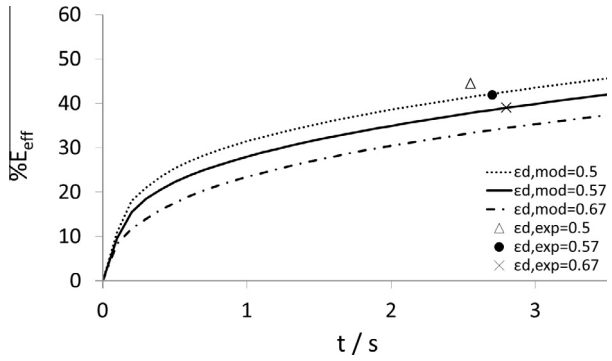

Fig. 10. Comparison of predicted extraction efficiencies of $\{UO_2\}^{2+}$ against the experimental ones as a function of the residence time (t) at three different volume fractions (ε_d) for constant Q_{mix} = 84.82 cm^3 h^{-1} in the 1 mm ID channel.

excess in the IL phase at all cases. As the dispersed phase volume fraction increases from 0.5 to 0.67, the plug length also increases while the interfacial area decreases by ~23%. This results to a smaller number of unit cells in the extractor and to a lower extraction efficiency as shown in Fig. 10. However, the amount of solvent used is reduced by 33.4%. Reduction in solvent use can be important for solvents such as ionic liquids which have high productions costs. Similar results were also obtained for the two other channel sizes (i.e., 0.5 and 2 mm ID). The experimental extraction efficiencies seem to agree well with those predicted by the simulations with a mean relative error for all conditions tested in the 3 channel sizes of about 11%.

5. Conclusions

The effect of channel size on the extraction of $\{UO_2\}^{2+}$ ions from nitric acid solutions into TBP/IL mixtures was studied during plug flow for channel sizes that varied from 0.5 to 2 mm ID. It was found that the extraction efficiency, which indicates how close to the equilibrium values the final concentrations are, and the mass transfer coefficient decrease as the channel size increases. The largest decrease in mass transfer coefficients occurred when the channel size changed from 0.5 to 1 mm ID while the decrease was less when the channel size changed from 1 to 2 mm ID. For a given channel length, extraction efficiencies decrease with mixture velocity in all channels studied, while the mass transfer coefficients increased moderately. In all channels it was found that significant extraction takes place as soon as the phases join at the inlet of the channel. For all conditions studied the mass transfer coefficients varied between 0.049 and 0.29 s^{-1}, which is in agreement with literature values for other small scale liquid–liquid contactors. A numerical model was developed, which used experimental data on the geometric characteristics of the plug flow and was able to predict the experimental extraction efficiencies reasonably well with an average relative error of 11%.

For increased throughput, scale out (or numbering up) is not sufficient as it would result to a very large number of very small channels, while a combination of increased size (scale up) and increased channel number (number up) is a better approach. In small scale processes where the two phases flow co-currently, the extraction performance of the device is limited by the equilibrium concentrations. However, the simple design of these systems aided by good separation of the phases at the end of each stage make possible a quasi-countercurrent approach to achieve high extraction efficiencies. A number of parameters would need to be considered to optimise this configuration, including among others, the channel size, the pressure drop, and the $\%E_{eff}$ reached in each stage.

Acknowledgements

The authors would like to acknowledge Prof. Kenneth R. Seddon and Dr. Natalia V. Plechkova of Queen's University Ionic Liquids Laboratories (QUILL) for providing the ionic liquids. The authors would also like to thank the Engineering and Physical Science Research Council UK (EPSRC) for providing the Photron Ultima APX high-speed camera for this work.

References

[1] G. Dummann, U. Quittmann, L. Gröschel, D.W. Agar, O. Wörz, K. Morgenschweis, The capillary-microreactor: a new reactor concept for the intensification of heat and mass transfer in liquid–liquid reactions, Catal. Today 79 (2003) 433–439.
[2] J. Swanson, Purex process flowsheets, Sci. Technol. Tributyl Phosphate 3 (1984) 55.
[3] N.V. Plechkova, K.R. Seddon, Applications of ionic liquids in the chemical industry, Chem. Soc. Rev. 37 (2008) 123–150.
[4] M. Freemantle, An introduction to ionic liquids, R. Soc. Chem. (2010).
[5] K. Binnemans, Lanthanides and actinides in ionic liquids, Chem. Rev. 107 (2007) 2592–2614.
[6] V. Dore, D. Tsaoulidis, P. Angeli, Mixing patterns in water plugs during water/ionic liquid segmented flow in microchannels, Chem. Eng. Sci. 80 (2012) 334–341.
[7] K.Y. Tung, C.C. Li, J.T. Yang, Mixing and hydrodynamic analysis of a droplet in a planar serpentine micromixer, Microfluid. Nanofluid. 7 (2009) 545–557.
[8] A. Gupta, R. Kumar, Flow regime transition at high capillary numbers in a microfluidic T-junction: viscosity contrast and geometry effect, Phys. Fluids (1994-present) 22 (2010) 122001.
[9] A. Gupta, S.S. Murshed, R. Kumar, Droplet formation and stability of flows in a microfluidic T-junction, Appl. Phys. Lett. 94 (2009) 164107.
[10] Y. Su, G. Chen, Q. Yuan, Effect of viscosity on the hydrodynamics of liquid processes in microchannels, Chem. Eng. Technol. 37 (2014) 427–434.
[11] J. Tan, J. Xu, S. Li, G. Luo, Drop dispenser in a cross-junction microfluidic device: scaling and mechanism of break-up, Chem. Eng. J. 136 (2008) 306–311.
[12] G.F. Christopher, N.N. Noharuddin, J.A. Taylor, S.L. Anna, Experimental observations of the squeezing-to-dripping transition in T-shaped microfluidic junctions, Phys. Rev. E Stat. Nonlin. Soft Matter Phys. 78 (2008) 036317.
[13] M.N. Kashid, D.W. Agar, S. Turek, CFD modelling of mass transfer with and without chemical reaction in the liquid–liquid slug flow microreactor, Chem. Eng. Sci. 62 (2007) 5102–5109.
[14] V. Dore, D. Tsaoulidis, P. Angeli, μ-PIV investigation of water/ionic liquid plug flow dynamics in meandering microchannels, in: 16th Int. Symp. on Applications of Laser Techniques to Fluid Mechanics, Lisbon, Portugal, 2012.
[15] F. Scheiff, A. Holbach, D.W. Agar, Slug flow of ionic liquids in capillary microcontactors: fluid dynamic intensification for solvent extraction, Chem. Eng. Technol. 36 (2013) 975–984.
[16] G. Berčič, A. Pintar, The role of gas bubbles and liquid slug lengths on mass transport in the Taylor flow through capillaries, Chem. Eng. Sci. 52 (1997) 3709–3719.
[17] J. Van Baten, R. Krishna, CFD simulations of mass transfer from Taylor bubbles rising in circular capillaries, Chem. Eng. Sci. 59 (2004) 2535–2545.

[18] S. Irandoust, B. Andersson, Liquid film in Taylor flow through a capillary, Ind. Eng. Chem. Res. 28 (1989) 1684–1688.
[19] C.O. Vandu, H. Liu, R. Krishna, Mass transfer from Taylor bubbles rising in single capillaries, Chem. Eng. Sci. 60 (2005) 6430–6437.
[20] J. Yue, L. Luo, Y. Gonthier, G. Chen, Q. Yuan, An experimental study of air–water Taylor flow and mass transfer inside square microchannels, Chem. Eng. Sci. 64 (2009) 3697–3708.
[21] N. Shao, A. Gavriilidis, P. Angeli, Mass transfer during Taylor flow in microchannels with and without chemical reaction, Chem. Eng. J. 160 (2010) 873–881.
[22] J.R. Burns, C. Ramshaw, The intensification of rapid reactions in multiphase systems using slug flow in capillaries, Lab Chip 1 (2001) 10–15.
[23] Y. Zhao, G. Chen, Q. Yuan, Liquid–liquid two-phase mass transfer in the T-junction microchannels, AIChE J. 53 (2007) 3042–3053.
[24] M.N. Kashid, Y.M. Harshe, D.W. Agar, Liquid–liquid slug flow in a capillary: an alternative to suspended drop or film contactors, Ind. Eng. Chem. Res. 46 (2007) 8420–8430.
[25] A.-L. Dessimoz, L. Cavin, A. Renken, L. Kiwi-Minsker, Liquid–liquid two-phase flow patterns and mass transfer characteristics in rectangular glass microreactors, Chem. Eng. Sci. 63 (2008) 4035–4044.
[26] Y. Su, Y. Zhao, G. Chen, Q. Yuan, Liquid–liquid two-phase flow and mass transfer characteristics in packed microchannels, Chem. Eng. Sci. 65 (2010) 3947–3956.
[27] A. Ghaini, M. Kashid, D. Agar, Effective interfacial area for mass transfer in the liquid–liquid slug flow capillary microreactors, Chem. Eng. Process. 49 (2010) 358–366.
[28] D. Tsaoulidis, V. Dore, P. Angeli, N.V. Plechkova, K.R. Seddon, Dioxouranium(VI) extraction in microchannels using ionic liquids, Chem. Eng. J. 227 (2013) 151–157.
[29] D. Tsaoulidis, V. Dore, P. Angeli, N.V. Plechkova, K.R. Seddon, Extraction of dioxouranium(VI) in small channels using ionic liquids, Chem. Eng. Res. Des. 91 (2013) 681–687.
[30] F. Sarrazin, T. Bonometti, L. Prat, C. Gourdon, J. Magnaudet, Hydrodynamic structures of droplets engineered in rectangular micro-channels, Microfluid. Nanofluid. 5 (2008) 131–137.
[31] N.D.M. Raimondi, L. Prat, Numerical study of the coupling between reaction and mass transfer for liquid–liquid slug flow in square microchannels, AIChE J. 57 (2011) 1719–1732.
[32] A.H.P. Skelland, R.M. Wellek, Resistance to mass transfer inside droplets, AIChE J. 10 (1964) 491–496.
[33] N. Harries, J.R. Burns, D.A. Barrow, C. Ramshaw, A numerical model for segmented flow in a microreactor, Int. J. Heat Mass Transf. 46 (2003) 3313–3322.
[34] N. Di Miceli Raimondi, L. Prat, C. Gourdon, P. Cognet, Direct numerical simulations of mass transfer in square microchannels for liquid–liquid slug flow, Chem. Eng. Sci. 63 (2008) 5522–5530.
[35] M. Kashid, A. Gupta, A. Renken, L. Kiwi-Minsker, Numbering-up and mass transfer studies of liquid–liquid two-phase microstructured reactors, Chem. Eng. J. 158 (2010) 233–240.
[36] D. Tsaoulidis, V. Dore, P. Angeli, N.V. Plechkova, K.R. Seddon, Flow patterns and pressure drop of ionic liquid–water two-phase flows in microchannels, Int. J. Multiph. Flow 54 (2013) 1–10.
[37] F. Scheiff, M. Mendorf, D. Agar, N. Reis, M. Mackley, The separation of immiscible liquid slugs within plastic microchannels using a metallic hydrophilic sidestream, Lab Chip 11 (2011) 1022–1029.
[38] M.N. Kashid, I. Gerlach, S. Goetz, J. Franzke, J.F. Acker, F. Platte, D.W. Agar, S. Turek, Internal circulation within the liquid slugs of a liquid–liquid slug-flow capillary microreactor, Ind. Eng. Chem. Res. 44 (2005) 5003–5010.
[39] M.L. Dietz, J.A. Dzielawa, Ion-exchange as a mode of cation transfer into room-temperature ionic liquids containing crown ethers: implications for the 'greenness' of ionic liquids as diluents in liquid–liquid extraction, Chem. Commun. (2001) 2124–2125.
[40] G.-T. Wei, Z. Yang, C.-J. Chen, Room temperature ionic liquid as a novel medium for liquid/liquid extraction of metal ions, Anal. Chim. Acta 488 (2003) 183–192.
[41] J. Tan, Y. Lu, J. Xu, G. Luo, Mass transfer characteristic in the formation stage of gas–liquid segmented flow in microchannel, Chem. Eng. J. 185 (2012) 314–320.
[42] D. Tsaoulidis, V. Dore, P. Angeli, Extraction of uranium in microfluidic channels using ionic liquids, in: Microfluidics 2012, Heidelberg, Germany, 2012.
[43] D. Tsaoulidis, Studies of intensified small-scale processes for liquid-liquid separations in spent nuclear fuel reprocessing (PhD thesis), University College London, 2014.
[44] C. Liu, J. Shang, J.M. Zachara, Multispecies diffusion models: a study of uranyl species diffusion, Water Resour. Res. 47 (2011).
[45] P. Giridhar, K. Venkatesan, T. Srinivasan, P. Rao, Electrochemical behavior of uranium (VI) in 1-butyl-3-methylimidazolium chloride and thermal characterization of uranium oxide deposit, Electrochim. Acta 52 (2007) 3006–3012.